Strain characterization of embedded aerospace smart materials using shearography

Andrei G. Anisimov*[a], Bernhard Müller[b], Jos Sinke[b], Roger M. Groves[a]
[a]Aerospace Non-Destructive Testing Laboratory, Delft University of Technology, Kluyverweg 1, 2629 HS, Delft, The Netherlands;
[b]Structural Integrity & Composites, Delft University of Technology, Kluyverweg 1, 2629 HS, Delft, The Netherlands

ABSTRACT

The development of smart materials for embedding in aerospace composites provides enhanced functionality for future aircraft structures. Critical flight conditions like icing of the leading edges can affect the aircraft functionality and controllability. Hence, anti-icing and de-icing capabilities are used. In case of leading edges made of fibre metal laminates heater elements can be embedded between composite layers. However this local heating causes strains and stresses in the structure due to the different thermal expansion coefficients of the different laminated materials. In order to characterize the structural behaviour during thermal loading full-field strain and shape measurement can be used. In this research, a shearography instrument with three spatially-distributed shearing cameras is used to measure surface displacement gradients which give a quantitative estimation of the in- and out-of-plane surface strain components. For the experimental part, two GLARE (Glass Laminate Aluminum Reinforced Epoxy) specimens with six different embedded copper heater elements were manufactured: two copper mesh shapes (straight and S-shape), three connection techniques (soldered, spot welded and overlapped) and one straight heater element with delaminations. The surface strain behaviour of the specimens due to thermal loading was measured and analysed. The comparison of the connection techniques of heater element parts showed that the overlapped connection has the smallest effect on the surface strain distribution. Furthermore, the possibility of defect detection and defect depth characterisation close to the heater elements was also investigated.

Keywords: Multicomponent shearography, strain measurement, defect depth characterisation, fibre metal laminates, GLARE, embedded heater elements, anti-icing, de-icing

1. INTRODUCTION

The development of smart materials for embedding in aerospace composites provides enhanced functionality for future aircraft structures[1]. For example, novel sensor networks that are embedded in composites can provide structural health monitoring (SHM) capabilities during the manufacturing and operational stages significantly broadening existing capabilities[2].

A critical flight condition is icing of the leading edges[3]. Icing of leading edges significantly changes the airflow and causes an increase in drag, a decrease in lift, and may affect the aircraft controllability[3]. Embedded heater elements in the leading edges of fibre metal laminate (FML) wing structures can provide anti-icing and de-icing capabilities[4]. However, the heating of leading edges of aircraft using embedded heater elements introduces strains and stresses in the structure due to the different thermal expansion coefficients of the different laminated materials[5, 6]. Thus, heating might affect the shape of the leading edges. The structural behaviour during thermal loading can be characterized using full-field strain and shape measurements. This research is the experimental part of the analysis of surface strain of GLARE with embedded heater elements. GLARE is an FML and the acronym for Glass Laminate Aluminum Reinforced Epoxy[7]. GLARE is a composite material with alternating layers of aluminum (2024-T3) and prepreg layers (S2 glass / FM94)[7].

In this research a multicomponent shearography (speckle shearing interferometry) instrument was used to measure surface displacement gradients which give a quantitative estimate of in- and out-of-plane surface strain components[8, 9]. These surface displacements are caused by resistance heating of the embedded heater elements. Thus, the strains due to thermal loading were measured and the results discussed. In a future step the experimental results will be used for the validation of numerical analyses of the stress-strain state during thermal loading.

*a.g.anisimov@tudelft.nl; phone +31 15 27 88233; http://www.aerondt.tudelft.nl

Sensors and Smart Structures Technologies for Civil, Mechanical, and Aerospace Systems 2015, edited by Jerome P. Lynch, Kon-Well Wang, Hoon Sohn, Proc. of SPIE Vol. 9435, 943524

· CCC code: 0277-786X/15/$18 · doi: 10.1117/12.2082636

2. GLARE SPECIMENS

For the experimental part, two GLARE 5-4/3-0.3 specimens with embedded heater elements were manufactured in a hand layup process where the embedded heater elements and K-type thermocouples were added. The GLARE specimens were manufactured by means of the standard method[5], i.e. by curing in an autoclave at temperatures of 120°C and a pressure of 6 bar. Figure 1 depicts the specimen dimensions and the heater element positions. The specimen dimensions are 800×550 mm and were chosen in order to avoid the possible disturbance from neighbouring heater elements or specimen edges on the measurement results[10]. Figure 2 shows the layup of the investigated GLARE 5-4/3-0.3 laminate with an overall thicknesses of 2.80 mm. The term GLARE 5-4/3-0.3 indicates that the laminate consists of four 0.30 mm thick aluminum layers and three prepreg layers[7]. Each prepreg layer consists of four 0.133 mm thick unidirectional glass fiber reinforced plastic layers with fiber orientations of 0° / 90° / 90° / 0°. The embedded heater elements were made of copper foil (Cu-OF, EN CW008A).

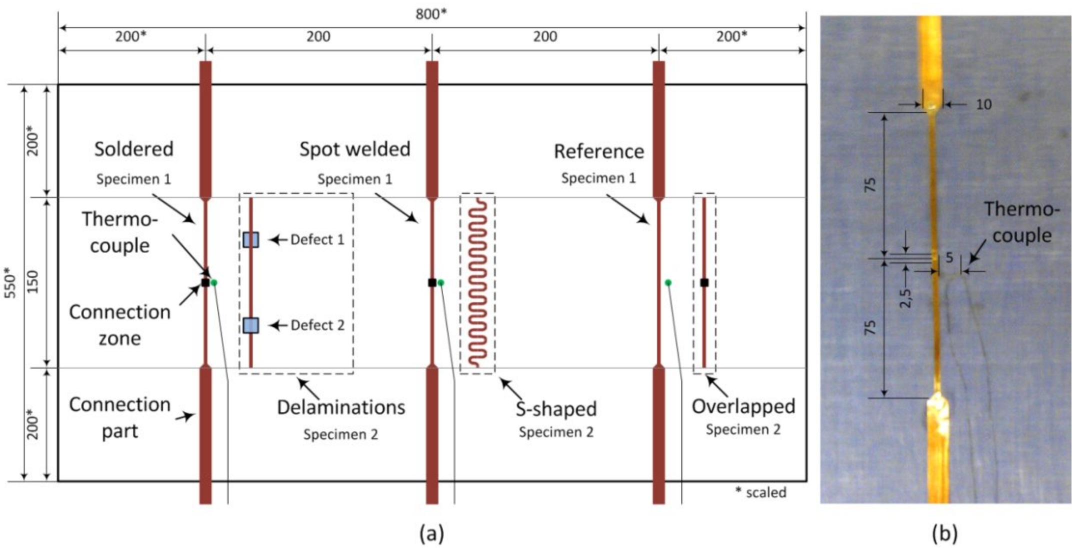

Figure 1. Specimens with embedded heater elements: (a) specimen dimensions and position of the heater elements; specimen 1 – main drawing, specimen 2 – parts in dashed rectangles and (b) photograph of the embedded spot welded heater element and thermocouple during the manufacturing.

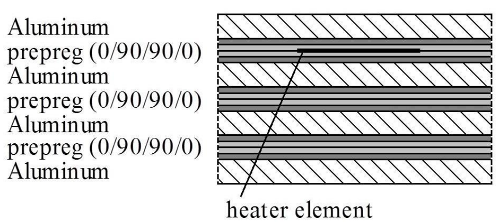

Figure 2. Heated GLARE 5-4/3-0.3 cross section.

Figure 1 (a) shows the geometries of the six different embedded copper heater elements of the two specimens. Two different copper mesh shapes (straight and S-shape), three different connection techniques (soldered, spot welded and overlapped) and one straight heater element with delaminations were manufactured. Figure 1 (b) depicts the positions of the heater element connections. The straight heater element was used as a reference as neither artificial delaminations nor connections were applied. The heater element width reduces from 10 mm to 2.5 mm along the 150 mm long center part to concentrate heating on the center part and to avoid heating the specimen outer parts to minimise edge effects. The thickness of the heater elements, except for soldered areas, remains constant and equals 0.125 mm. The fiber orientation of the prepreg layers next to the heater elements (in Figure 2 they are indicated as 90°) agrees with the heater element orientation.

Artificial delaminations were introduced by placing two polytetrafluoroethylene (PTFE) foil pieces of 5×5 mm between the heater element and the next two prepreg layers during the layup[11]. The artificial delamination positioned between the heater and inner prepreg layer is referred to defect 1 and the delamination between the heater and outer prepreg layer is referred to defect 2 (see Figures 1 (a) and 2). Furthermore, thermocouples were positioned at a distance of 5 mm to the right of each heater element in order to measure and control the temperature between the two prepreg layers next to heater elements. Figure 1 (b) depicts the position of one of the thermocouples.

3. SHEAROGRAPHY THEORY

Shearography uses laser speckle interferometry to provide a direct measurement of the surface displacement gradients which give a quantitative estimate of in- and out-of-plane surface strain components[8, 9]. During measurements the speckle pattern is generated by illuminating the object with an expanded laser beam. The object is imaged with a camera with a shearing device to obtain interferograms before and after loading. The shearing device duplicates camera field of view with a small shearing one from another to bring two surface points $P(x, y, z)$ and $Q(x, y+dy, z)$ (Figure 3) to one point on the camera sensor. These points are separated by the shear distance dy and belong to the surface at the initial state. At this state a reference interferograms are recorded and a phase-shift algorithm[12] is used to get the difference of phase at each camera pixel $\phi^{initial}$.

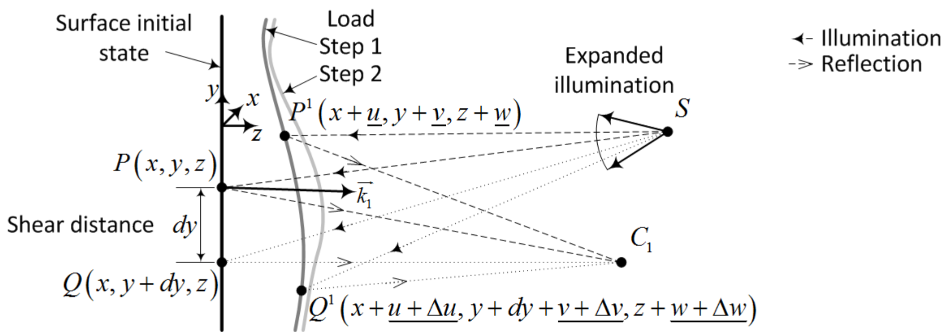

Figure 3. Schematic representation of optical paths differences in shearography.

After the first step of thermal loading (expansion due to thermal expansion coefficients[5]) the points P and Q move to their new positions P^1 and Q^1, respectively, and a signal interferograms are recorded to get the signal difference of phase at each camera pixel ϕ^1. The expansion causes a change in optical path length[9] ΔL^1 between the laser located at S, the first camera located at C_1 and the surface points P, P^1, Q, Q^1:

$$\Delta L^1 = \left(SP^1C_1 - SPC_1\right) - \left(SQ^1C_1 - SQC_1\right) = k_{x1}\Delta u + k_{y1}\Delta v + k_{z1}\Delta w \tag{1}$$

where $[k_{x1}\ k_{y1}\ k_{z1}]$ are components of the sensitivity vector $\overrightarrow{k_1}$ of camera 1, that is the bisector between the illumination $\overrightarrow{PS}$ and viewing $\overrightarrow{PC_1}$ directions. The displacement (u, v, w) and displacement difference $(\Delta u, \Delta v, \Delta w)$ are given in the (x, y, z) coordinate system.

For a small amount of shear in the y-direction dy_1 ($dy_1 \ll PC_1$ and $dy_1 \ll PS$) the phase change $\Delta\phi_{y1}^1$ at camera 1 is caused by the change in optical path length ΔL^1 and can be calculated as a function of the surface strain components $(\partial u/\partial y, \partial v/\partial y, \partial w/\partial y)$ using[9]:

$$\Delta\phi_{y1}^1 = \phi_{y1}^1 - \phi_{y1}^{initial} = \frac{2\pi}{\lambda}\left(k_{x1}\,\partial u/\partial y + k_{y1}\,\partial v/\partial y + k_{z1}\,\partial w/\partial y\right)dy_1 \tag{2}$$

where $\phi_{y1}^{initial}$ and ϕ_{y1}^1 are the reference and signal phase differences obtained at camera 1 at the initial surface state and after the first load step, respectively, λ is the laser wavelength.

In order to isolate the surface strain components a multicomponent shearography instrument with three viewing directions (three cameras) can be used[13, 14]. The surface strain components $(\partial u/\partial y, \partial v/\partial y, \partial w/\partial y)$ for the shear in the y-direction can be calculated[15] by processing phase changes $\Delta\phi_{yj}$ obtained at each camera j ($j = 1, 2, 3$):

$$\begin{bmatrix} \partial u/\partial y \\ \partial v/\partial y \\ \partial w/\partial y \end{bmatrix} = \frac{\lambda}{2\pi}\begin{bmatrix} k_{x1} & k_{y1} & k_{z1} \\ k_{x2} & k_{y2} & k_{z2} \\ k_{x3} & k_{y3} & k_{z3} \end{bmatrix}^{-1}\begin{bmatrix} \Delta\phi_{y1}/dy_1 \\ \Delta\phi_{y2}/dy_2 \\ \Delta\phi_{y3}/dy_3 \end{bmatrix} \tag{3}$$

where $[k_{xj}\ k_{yj}\ k_{zj}]$ are components of the sensitivity vector and dy_j is the shear distance of each camera j. The surface strain components in the x-direction $(\partial u/\partial x, \partial v/\partial x, \partial w/\partial x)$ can be calculated in the same way[13] replacing y by x in Equations (2-3).

In order to obtain the surface strain components after total deformation two ways are possible[16]. One option is to calculate the total phase change $\Delta\phi$ for each camera and shear direction:

$$\Delta\phi = \left(\phi^1 - \phi^{initial}\right) + \left(\phi^2 - \phi^1\right) + \ldots + \left(\phi^{last\ step} - \phi^{last\ step-1}\right). \tag{4}$$

In Equation (4) the subscript of ϕ indicating the camera number and the shear direction is omitted for clarity.

The second option is to calculate the surface strain components for each load step and then to sum them up, like for $\partial u/\partial y$:

$$\partial u/\partial y = \partial u/\partial y^1 + \partial u/\partial y^2 + \ldots + \partial u/\partial y^{last\ step}. \tag{5}$$

In order to get the absolute values of the surface strain components both options require the identification of the zero order fringe (zone of phase distribution corresponding to a zero surface displacement) during the phase unwrapping procedure, if the phase change exceeds the $[0, 2\pi]$ or $[-\pi, \pi]$ ranges during a load step. Apart from the S-shaped heater element, the heater elements used in this research are symmetric with respect to their yz-plane (cf. Figures 1, 3). Therefore, symmetric strain distributions in respect to the heater elements are expected and the zero order fringe was chosen to be aligned with the heater centres.

To get a reliable strain components estimation, the coordinate transformation (Equation (3)) should be performed pixel by pixel in the ROI using a sensitivity matrix and shear maps correction[16]. For a high number of load steps it takes a significant time to process all the data. Therefore, the total phase map technique is preferable as it enables a faster calculation. The disadvantage is that it does not allow the tracking of the surface strain components in respect to time.

4. MULTICOMPONENT SHEAROGRAPHY INSTRUMENT

A multicomponent shearography instrument with multiple viewing and single illumination configuration was developed for the experimental research (see Figure 4). Three spatially-distributed shearing cameras and the laser were placed in cross configuration using an Alufix modular fixture system[17]. The cameras were calibrated in pairs as stereovision systems to give an accurate estimation of cameras location and imaging lenses distortion correction[18, 19]. Shearing cameras consist of Basler Pilot piA2400 cameras with Linos MeVis-C 1.6/25 imaging lenses and shearing devices based on Michelson interferometers[20, 21].

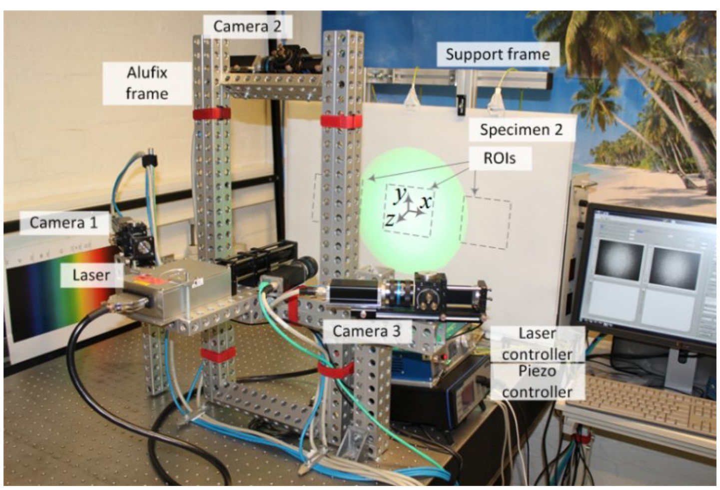

System configuration, mm

	x	y	z
Laser	11	5	550
Camera 1	−291	−59	653
Camera 2	48	332	547
Camera 3	434	−37	645

The coordinate system origin is in the ROI center

Figure 4. Multicomponent shearography system with calibrated system configuration parameters

Image shearing and temporal phase-shifting is performed by control of one of the mirrors in each interferometer by a three coordinate piezo-electric actuator. Actual shearing distances were calibrated for the region of interest (ROI) for each camera and formed actual shear maps with mean value close to 1 mm. Figure 4 depicts the ROIs used in this study as a squares marked with dashed lines. A ROI size was chosen to be 120×120 mm for each heater element. The heater elements were positioned in the ROI center. The specimen was positioned in front of the shearography instrument at a working distance of 500 mm and clamped to a support frame in its four corners.

The heater temperature may reach 70°C during in-flight operation[22]. The deformation magnitude arising during this heating is quite significant for measuring using shearography. Therefore, a high dynamic range of the shearography instrument is required to record the arising strains. In order to reduce the required dynamic range a sequential measuring in several thermal load steps with temporal phase-shifting technique was employed[9]. A simple three-step phase shifting technique is the fastest in comparison with higher number of steps, because of the minimal number of piezo movements and images to be taken and was chosen for the sequential measurements[12, 23].

5. SURFACE STRAIN BEHAVIOUR DURING THERMAL LOADING

5.1. Thermal loading

Thermal loading is realised through resistance heating of the embedded heater elements. A constant power of 22 W was applied. Figure 5 depicts the temperature curve due to this thermal loading. The curve was measured with the thermocouple positioned next to the spot welded heater element (see Figure 1 (b)). The initial temperature equals the room temperature and rises within 120 s to 39°C.

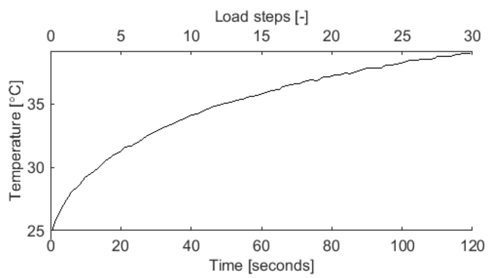

Figure 5. Temperature increase due to thermal loading over time as measured using the thermocouple.

5.2. Measured surface strain components

The shearography instrument used in this study is limited to a data acquisition time of every 4 seconds because of the piezo-electric actuators settling time and the camera frame rate. Thus, 30 measurements were taken and the resultant phase maps were calculated using Equation (4) in a post processing step for the spot welded heater element for the temperature increase after 120 s (cf. Figure 5).

After that the six resultant surface strain components were calculated using Equation (3) (Figure 6). The surface strain components $\partial v/\partial x, \partial w/\partial x, \partial u/\partial y, \partial w/\partial y$ are depicted in Figures 6 (a-d). The three surface strain components $\partial u/\partial x$, $\partial v/\partial y$ and $\gamma_{xy} = (\partial u/\partial y + \partial v/\partial x)$ which are commonly used for the assessment of stress-strain states are enlarged and shown in Figure 6 (e-g). Furthermore, Figures 6 (h-j) depict the lateral surface strain components across the ROI.

The strain component $\partial u/\partial x$ (Figure 6 (e, h)) shows that in the x-direction the material expands in regions close to the heater element and compresses in regions further away. The strain distribution in the x-direction is almost symmetric in respect to the heater element.

The strain component $\partial v/\partial y$ (Figure 6 (f, i)) shows that in the y-direction large regions compress. Those compressive strains result from the bending of the specimen due to thermal loading. The specimen center (spot weld) shifts from its initial positon backwards in the negative z-direction. This backward bending could be clearly seen during the thermal loading.

5.3. Heater elements connection

The effect of different connection techniques (spot welded, soldered and overlapped) on the surface strain distribution was analysed. Each heater element was thermally loaded in the same way as depicted in Figure 5. Figure 6 shows, that the effect of the spot welded heater on the strain distributions is visible in all six surface strain components, but the out-of-plane strain components are most affected and the effect of heater connection can be seen clearly. Therefore, Figure 7 focuses on the out-of-plane strain components of the different connection techniques.

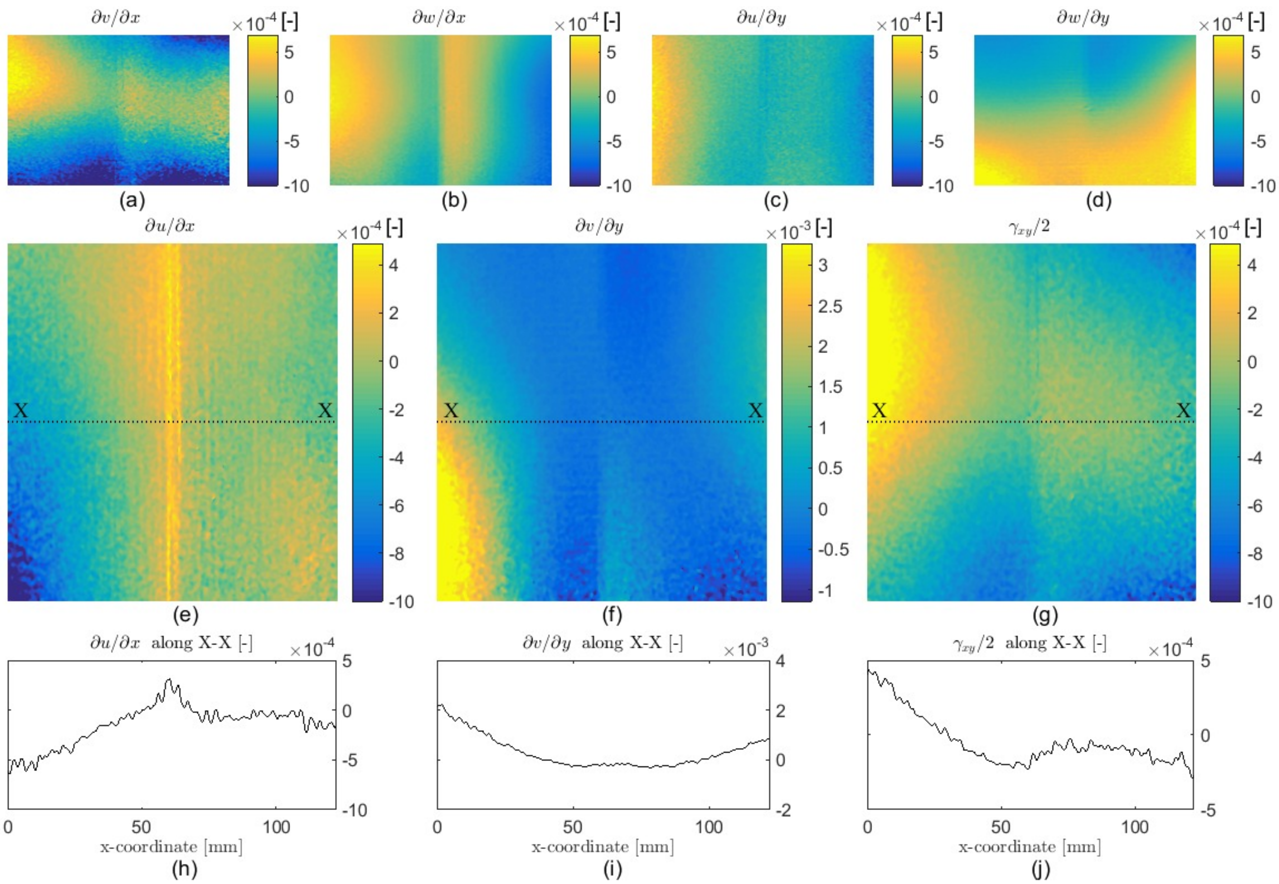

Figure 6. Surface strain components for the spot welded heater element: (a-g) strain maps across the surface in the ROI 120×120 mm (1062×1040 pixels) and (h-j) surface strain components along X-X.

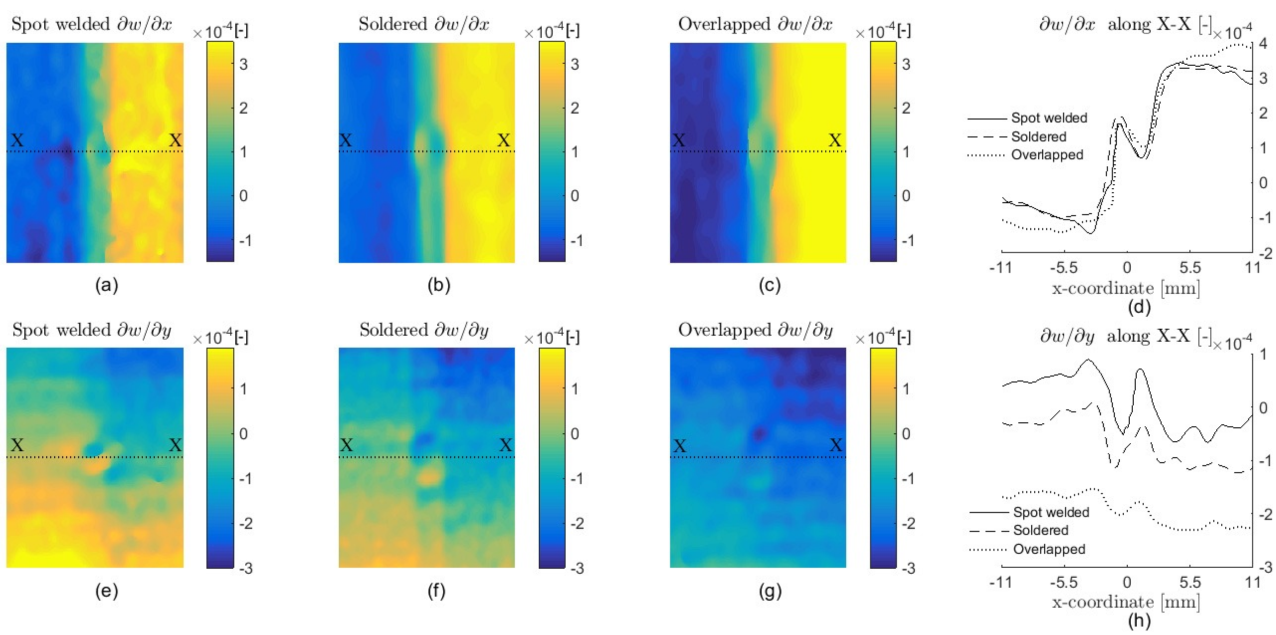

Figure 7. Out-of-plane surface strain components of the (a, e) spot welded, (b, f) soldered and (c, g) overlapped heater element connections. The depicted areas in (a-c) and (e-g) are 22×22 mm (200×200 pixels). (d, h) are the surface strain components along X-X.

According to the results, the overlap connection technique (cf. Figure 7 (d, h)) affects the strain distribution less than soldering or spot welding. Thus, the local thickness variations of the connection parts mainly affect the out-of-plane surface strain component behaviour. Figure 7 shows that differences in the strain distributions can be seen most clearly by processing the $\partial w/\partial y$ component. The strain component $\partial w/\partial y$ of the overlapped connection, the soldered and the spot welded specimen differ about 1×10^{-4} and 2×10^{-4}, respectively. The overlap was done by simple overlapping of the heater element parts without any mechanical connection. This resulted in the minimal overall thickness of the connection region as neither additional material was added (soldering) nor local heater element deformation due to the concentrated heat input (spot welding).

5.4. Defect detection and characterization

The characterisation and classification of defects, i.e. delamination types was investigated by measuring the out-of-plain strain components. Similarly to the previous section, the out-of-plane stain components showed the possible effects of delaminations on the strain distribution most clearly. Figure 8 depicts the out-of-plane strain in the vicinity of the two delaminations depicted in Figure 1(a).

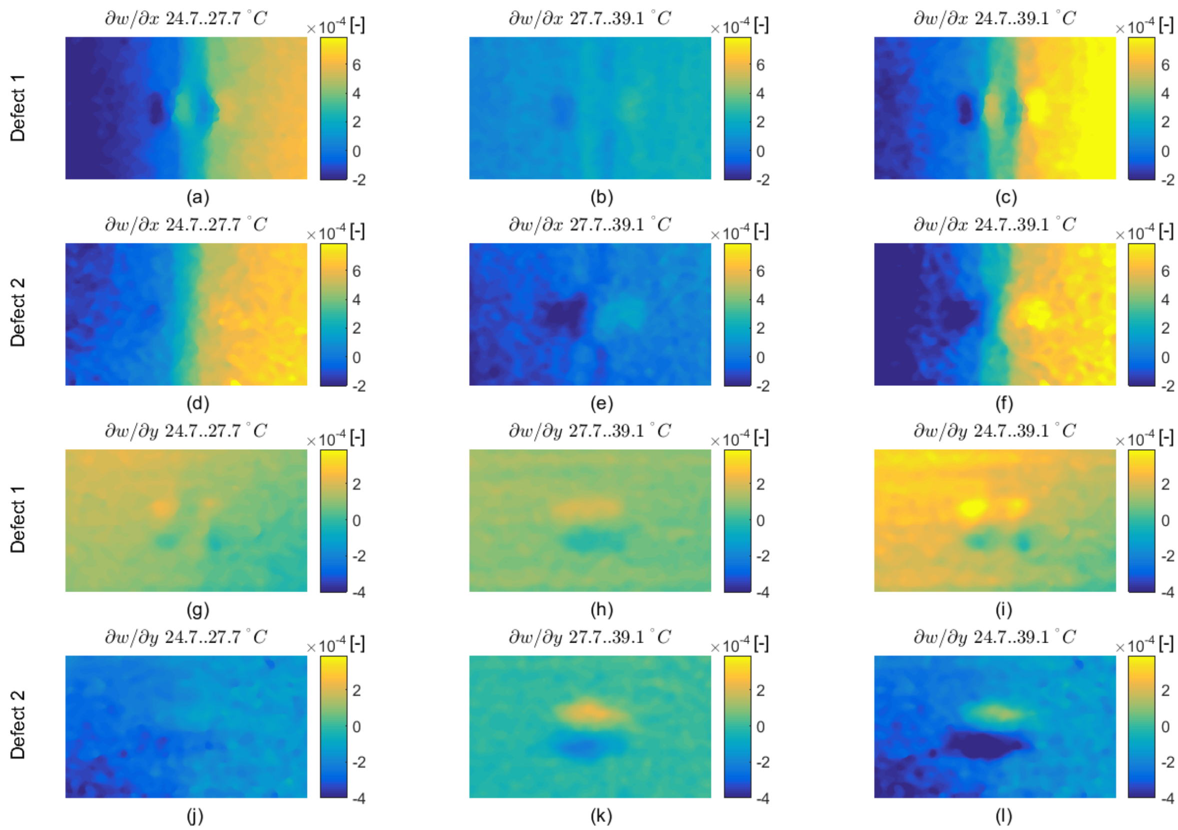

Figure 8. Defect detection in FML. Out-of-plane strain components for different temperatures. First and second row: $\partial w/\partial x$ for defect 1 (a-c) and defect 2 (d-f). Third and fourth row: $\partial w/\partial y$ for defect 1 (g-i) and defect 2 (j-l). The depicted areas are 28×18 mm (240×160 pixels).

In order to show the effects of delaminations on the strain distributions more clearly, the surface strains shown in Figure 8 were calculated for the temperature differences of 24.7 to 27.7°C (first column), 27.7 to 39.1°C (second column) and the total temperature range of 24.7 to 39.1°C (third column). Figure 8 (a) shows that the defect 1 (delamination between the heater and inner prepreg layer) can be identified by analysis of the strain component $\partial w/\partial x$ obtained between 24.7 and 27.7°C. While the effects caused by defect 2 (delamination between the heater and outer prepreg layer) are revealed most clearly during the remaining heating range from 27.7 to 39.1°C (Figure 8 (e)). The total strain variation for both defects varies between -2×10^{-4} and 6×10^{-4} (third column) and therefore does not reveal any difference between the defects. Similarly to the strain component $\partial w/\partial x$, the changes of the strain component $\partial w/\partial y$ indicate possible defects as well (Figure 8 (g-l)).

6. DISCUSSION

The assumption made about the zero order fringe aligned with the heater centres agrees for displacements in the x-direction as the distribution of the $\partial u/\partial x$ train component is symmetric in respect to the yz-plane and to the heater element (cf. Figure 6 (e, h)). Contrary to the strains in the x-direction, tracking of the zero order fringe for strains in the y-direction is more complicated because the strain distribution across the heater y-axes is not always aligned with the heater center. The shearography instrument configuration used in the paper consists of three cameras (see Figure 3) as this is the minimal number to isolate the surface strain components[13]. Known techniques of employing one or more additional viewing directions may be used in the future to track the zero order fringe automatically[24, 25].

The bending of specimen 1 with the spot welded heater element in the negative z-direction was not expected (cf. Figure 3 and 6). Due to the asymmetric layup and the expected asymmetric temperature distribution across the xy-plane, the specimens were expected to bend in the positive z-direction. The bending in the negative z-direction is most probably a result of pre-stresses introduced during the manufacturing process. Those pre-stresses are expected to influence deformations during thermal loading. This finding is especially important for future research, as one of the aims of the shearography measurements is to provide experimental surface strain data of heated GLARE due to thermal loading for the validation of future finite element analyses.

Results obtained for the surface strain of different connection techniques show that the minimization of connection zone thickness together with its flatness result in minimal surface strain during the heating. The spot welding technique causes local surface disturbances that result in the highest strain variation (up to 10^{-4}) compared to the soldered and overlap connections (cf. Figure 7 (h)).

Detection of manufacturing and operational defects and damages in FML is an current topic in aerospace non-destructive testing (NDT)[26]. Possible delaminations between heater elements and prepreg layers could beside of changing the mechanical properties of the laminate also have a significant effect in misbalancing the local heat propagation. Two types of delaminations may take place:

- delamination between the heater and inner prepreg layer (Figure 1, defect 1) limits heat propagation to the material depth; this causes an overheat of the outer prepeg layers. If the heater temperature is more than the GLARE curing temperature this may cause irreversible material structure changes.
- delamination between the heater and outer prepreg layer (Figure 1, defect 2) limits heat propagation to the material outer surface that causes unheated zones with decreasing of anti-icing or/and de-icing reliability.

The presented results in NDT of heated GLARE (Figure 8) show that delaminations between the heater and prepreg layers can be detected and classified using multicomponent shearography. However, the resultant strain value caused by the defect and its shape can be used only for the defect detection. This classification significantly depends on the defect shape. For example defect 1 (Figure 1 (a)) has a symmetric shape in respect to the heater y-axes that causes symmetric distribution of the surface strain (Figure 8 (c, i)). If the defect 1 had a one sided location or more complicated shape it may act as a single "bubble" and could be mixed up with the defect 2 during analysis (Figure 8 (f, l)). Additional information about the strain growth in time during the sequential load steps (Figure 8 (a, g) for defect 1 and (e, k) for defect 2) provides sufficient information for a reliable delamination classification in order to choose a proper treatment or repair.

7. CONCLUSIONS

This study covers shearography surface strain characterization of heated GLARE due to thermal loading. A straight heater element without any artificial defects was used as a reference heater element. The following conclusions were drawn by comparing the strain distributions of the reference heater element with those from heater elements with artificial connections or delaminations.

Three different connection techniques (soldering, spot welding and overlap) of heater parts inside of the material were investigated. Comparison of the measured strain distributions showed that the out-of-plane strain components $\partial w/\partial x$ and $\partial w/\partial y$ are most affected by the different connection techniques. Furthermore, the results show that the overlapped connection has the smallest effect on the strain distribution compared to the soldered and spot welded specimen.

The possibility of defect detection of artificial delaminations at both sides of heater elements using shearography was examined. The results show that the out-of-plane strain components are most affected and therefore can be used for the detection and depth characterisation of defects. The two types of artificial delaminations (between heater and inner and outer prepreg layers) could be distinguished using multicomponent shearography.

All of the presented results prove that the multicomponent shearography technique is capable of measuring six in- and out-of-plane surface strain components can be used for advanced strain characterization of heated GLARE and embedded aerospace smart materials.

For future research the shearography instrument may be developed by employing additional viewing directions for robust absolute phase and consequently, absolute strain reconstruction. This is important for a future experimental analysis of heater elements with more complex shapes. At the same time the strain distribution due to higher temperature increase rates (e.g. 60°C within 10 s) is a topic of interest. Higher temperature increase and cooling rates require an increase of cameras frame rate together with high-speed shearing and phase shifting devices.

The next step of this research is to use the presented experimental results to validate coupled-thermal analyses. After the validation of the numerical analysis, different thermal loading conditions, the heater element patterns and positions will be examined.

ACKNOWLEDGMENTS

This study is partially funded by the Dutch research agency Technology Foundation (STW), Fokker Aerostructures and by the Skolkovo Institute of Science and Technology (Russia).

REFERENCES

[1] Vermeeren, C., (ed.), [Around Glare – a new aircraft material in context], Dortrecht: Kluwer Academic Publishers (2002).
[2] Speckmann, H., and Roesner, H. "Structural health monitoring: A contribution to the intelligent aircraft structure," Proceedings of ECNDT (2006).
[3] Thomas, S.K., Cassoni, R.P., "Aircraft anti-icing and de-icing techniques and modelling," Journal of Aircraft 33, 841-854 (1996)
[4] FMLC, Fibre Metal Laminates Centre of Competence, http://www.fmlc.nl/researchdevelopment/innovation/ (2014).
[5] Hagenbeek, M., [Characterisation of Fibre Metal Laminates under Thermo-mechanical Loadings], PhD-thesis, Delft University of Technology, Netherlands (2005).
[6] Hofslagare, P.,"Residual Stress Measurement on Fibre-metal-laminates," Journal of Neutron Research, Vol. 11(4), pp. 215-220 (2003).
[7] Vlot, A., and Gunnink, J.W., [Fibre Metal Laminates – An Introduction], Dortrecht: Kluwer Academic Publishers (2001).
[8] Hung, Y.Y., "Shearography: a new optical method for strain measurement and non-destructive testing," Opt. Eng. 21, 213391 (1982).
[9] Steinchen, W., Yang, L., [Digital Shearography], SPIE Press, Bellingham, Washington (2003).
[10] Müller, B., Teixeira De Freitas, S., Sinke, J., "Measuring thermal diffusion in fiber metal laminates," Proceedings of ICAST2014: 25nd International Conference on Adaptive Structures and Technologies, The Hague, 76 (2014).
[11] Krishnapillai, M., Jones, R., Marshall, I.H., Bannister, M., Rajic, N., "NDTE using pulse thermography: Numerical modeling of composite subsurface defects," Composite Structures 75(1-4), 241-249 (2006)
[12] Dorrio, B.V., and Fernandez J.L., "Phase-evaluation methods in whole-field optical measurement techniques," Meas. Sci. Technol. 10, R33-R35 (1999).
[13] James, S.W., Tatam, R.P., "Time-Division-Multiplexed 3D Shearography," Proc. SPIE 3744, 394-403 (1999).
[14] Groves, R.M., James, S.W., Tatam, R.P., "Multi-component shearography employing four measurement channels," Proc. SPIE 4933, 135-140 (2003).

[15] Francis, D., James, S.W., Tatam, R.P., "Surface strain measurement using multi-component shearography with coherent fibre-optic imaging bundles," Meas. Sci. Technol. 18(11), 3583 (2007).
[16] Goto, D.T., Groves, R.M., "A combined experimental with simulation approach to calibrated 3D strain measurement using shearography," Proc. SPIE 7387, 77871J (2010).
[17] Alufix modular fixture system, http://www.horst-witte.de/en/products/modular-fixturing-systems/alufix-classic.php (2015)
[18] Bouguet, J.Y., "Camera calibration toolbox for matlab," (2004).
[19] Heikkila, J., & Silvén, O., "A four-step camera calibration procedure with implicit image correction," In Computer Vision and Pattern Recognition, Proceedings IEEE Computer Society Conference, 1106-1112 (1997).
[20] Basler pilot family, http://www.baslerweb.com/en/products/area-scan-cameras/pilot/ (2015).
[21] LINOS Machine Vision Lenses, http://www.qioptiq-shop.com/en/Precision-Optics/LINOS-Machine-Vision-Solutions/LINOS-Machine-Vision-Lenses/MeVis-C.html/ (2015).
[22] Mohseni, M., Amirfazli, A., "A novel electro-thermal anti-icing system for fiber-reinforced polymer composite airfoils," Cold Regions Science and Technology 87, 47-58 (2013)
[23] Francis, D., Tatam, R.P., Groves, R.M., "Shearography technology and applications: a review," Meas. Sci. Technol. 21, 102001, 29 (2010).
[24] Siebert, T., Splitthof, K., Ettemeyer, A., "A practical approach to the problem of the absolute phase in speckle interferometry," Journal of Holography and Speckle 1(1), 32-38 (2004).
[25] Charrett, T., Francis, D., Tatam, R., "Quantitative shearography: error reduction by using more than three measurement channels," Appl. Opt. 50, 134-146 (2011).
[26] Dragan, K., Kornas, L., Kosmatka, M., Leski, A., Sałaciński, M., Synaszko, P., Bieniaś, J., "Damage Detection and Size Quantification of FML with the Use of NDE," Fatigue of Aircraft Structures 4, 5-9 (2012).